

Examination of Calcium-Phosphates Prepared from Eggshell

Csaba Balázs^{1a}, Zsuzsanna Kövér^{1b}, Enikő Horváth^{2d},
Csaba Németh^{3e}, Zsolt Kasztovszky^{4f}, Sándor Kurunczi^{5g}, Ferenc Wéber^{1c}

¹Ceramics and Composites Laboratory, Research Institute for Technical Physics and Materials Science, Hungary, H-1525 Budapest, P.O. Box 49,

²Laboratory for Nanostructures Research, Research Institute for Technical Physics and Materials Science, Budapest, Hungary,

³Institute of Isotope and Surface Chemistry, Chemical Research Center, Hungary, H-1525 Budapest, P.O. Box 77.,

⁴Department of Nuclear Research, Institute of Isotope and Surface Chemistry, Chemical Research Center, Budapest, Hungary,

⁵Nanosensorics Laboratory, Research Institute for Technical Physics and Materials Science, Hungary, H-1525 Budapest, P.O. Box 49.

^aemail: balazsi@mfa.kfki.hu, ^bemail: koverzs@mfa.kfki.hu, ^cemail: weber@mfa.kfki.hu,
^demail: horvathe@mfa.kfki.hu, ^eemail: nemeth@iserv.iki.kfki.hu, ^femail: kzsolt@alpha0.iki.kfki.hu,
^gemail: kurunczi@mfa.kfki.hu

Keywords: eggshell, calcium phosphates, hydroxyapatite, nanograins, biocomposites

Abstract. Calcium phosphates and hydroxyapatite nanopowders have been produced by using eggshell derived raw materials and phosphoric acid at different mixing ratios. The characteristics of the end product have been found to be influenced by acid/CaO mixing ratio, milling time and heat treatment applied. Calcium phosphate foams resulted at higher acid/CaO mixing ratio with high specific surface area. Compositional analyses showed that the Ca/P atomic ratios of the calcium phosphate foams are significantly smaller than for hydroxyapatite samples. At higher sintering temperatures calcium phosphate thin and thick film coatings have been produced by a condensation method. The calcium phosphate thin films consist of micron size crystals and nanofibrous layers.

Introduction

In this work the preparation of hydroxyapatite (HAP) and other calcium phosphates from biogenic (natural) materials is presented. Hydroxyapatite (HAP) is known as a highly bioactive and biocompatible inorganic material which helps bone regeneration [1,2]. Therefore, it is widely used in tissue engineering and bone replacement [3,4]. In this study calcium phosphate based bioceramics were synthesized by using eggshell derived raw materials and phosphoric acid. The phosphoric acid was added to starting powders at different mixing ratios. In order to get the full use of the benefits provided by high percentage of calcium carbonate in eggshell it is crucial to improve the synthesis processes. Due to unfavourable mechanical properties that were reported for porous HAP and calcium phosphate based ceramics [5], importance was given to composite processing. Different methods are known for calcium-phosphate coating processing, such as electrophoretic deposition [6], sol-gel [7], sputtering [8] or plasma spray [9]. A specific biomimetic process for apatite coating was presented by Kokubo et al. [10]. In present study, first the calcium-phosphate substrates were prepared. After that, a condensation method was applied to produce calcium phosphate coating. In this paper the preparation and coating processes as well as morphological and structural observations are presented.

Experimental procedure

Preparation of powders

Raw eggshells were calcinated at 900°C. After a short time (30 min.) the colour of eggshells turned to black, and after 3 hours they became white. The colour change suggested that most of the organic materials were burnt out. As-obtained powders were crushed in an agate mortar and reacted with phosphoric acid by an exothermic reaction. The details of mixing procedure and powder preparation are presented in Table. 1. Short (10 hours) and long milling (24 hours) times were applied. For example, powder sample A resulted from short milling, whereas the powder sample B, which is a derivative product of sample A, was obtained from long milling. Sample B contains double amount of phosphoric acid. All of the products that derived from powder samples A and B have notations as „S” (A sintered, noted AS), „P” (contains polyethylenglycol), „PS” (contains PEG and sintered) or „BCPS” (powder B contains carbon „C”, PEG and sintered). After milling, polyethylenglycol (PEG) was added to some of the powder mixtures. The batches were sieved with 100 µm mesh. Green samples were obtained by dry pressing at 220 MPa.

Table 1. The details of mixing procedure and powder preparation

Samples	Starting powders (eggshell)	H ₃ PO ₄	Carbon addition to batch	PEG addition to batch	Ball milling (in ethanol)	Sintering conditions	
		wt%	wt%	wt%		wt%	Temp.(°C)
A	50	50	-		10h	-	-
AS	50	50	-		10h	900°C	2h
APS	50	50	-	10	10h	1000°C	2h
B	derivative to A, 50	50	-		24h	-	-
BPS	50	50	-	10	24h	900°C	2h
BCP	50	50	1	10	24h	-	-
BCPS	50	50	1	10	24h	900/1000°C	2h

Sintering method

Sintering of samples was performed in air at 900°C or 1000°C for two hours. The heating rate did not exceed 2°C/min. The dimensions of the as-sintered specimens were 3.5 x 5 x 50 mm or bigger (in the case of series of B).

Microstructure and mechanical properties

Phase compositions were determined by Philips PW 1050 diffractometer. Morphology of the solid products was studied by field emission scanning electron microscope, LEO 1540 XB.

Compositional analysis

The total reflection x-ray fluorescence (TXRF) spectrometer was calibrated using dilute solutions of commercially available standards. Single element stock solutions (1000 ppm) were purchased from Spectrascan, and subsequently diluted using Milli-Q water (REWA HQ-5). An amount of ~ 10 mg of the apatite fine powder was precisely measured into plastic flask (25 ml), then dissolved in diluted nitric acid solution. The process of dissolution was amplified by means of ultrasonic bath. Finally, Cr stock solution was added so that the concentration was set to 40 ppm for Cr as the internal standard. A volume of 5 µl of solution was pipetted on the Plexiglass reflectors and dried in laminar air flow. The very thin film remained after the drying represents the specimen to be measured by TXRF spectrometry. The x-ray generator (Mo-anode tube) was operated at 50 kV high

voltage and 20 mA current. The TXRF spectrometer has been installed and used previously for inorganic analysis [11]. The old set up was used with a slight modification of the detection. The excited characteristic x-rays were detected with a novel Si drift detector [12]. High voltage (180 V), and power supply for Peltier cooling were plugged in the detector. The energy resolution of the KETEK detector was FWHM= 160 eV at 5.9 keV. Signals were processed (Canberra 2025 amplifier, 1 μ s shaping), and collected by the Genie 2000 ADC/MCA PC card and software. Spectra were evaluated by the QXAS software package [13].

The second method for compositional analyses was prompt gamma activation analysis (PGAA). PGAA is based on the detection of gamma-ray photons, which are emitted after the capture of thermal or sub-thermal neutrons into the atomic nuclei, i.e. the (n, γ) reaction. The photon energies range between 50 keV and 11 MeV and are characteristic for a given element. The element identification is based on the precise determination of gamma photon energies and intensities. For PGAA analysis a guided cold neutron beam was used, obtained from the 10 MW Budapest Research Reactor. The thermal neutrons, which exit the reactor core, were cooled by a liquid hydrogen cell down to 16 K. Consequently, the achieved thermal equivalent neutron flux was $5 \cdot 10^7 \text{ cm}^{-2} \text{ s}^{-1}$. The size of the neutron beam was $2 \times 2 \text{ cm}^2$. The investigated samples were packed in thin FEP films, and were placed in a well-defined position of the sample holder chamber. In order to reduce the background caused by neutrons, which captured or scattered on air, the vacuum chamber was evacuated to 10^{-1} mbar. A complex HPGe-BGO detector system was used in order to perform a Compton-suppressed detection mode of γ -photons. The signals were processed with a multi-channel analyzer, then the spectra were evaluated with Hypermet-PC software; the element identification was performed on the basis of prompt-gamma database. The details of standardization procedure are described by Révay and Molnár [14].

Results and discussion

After calcination at 900°C, 3 hours the main lines of $\text{Ca}(\text{OH})_2$ (JCPDS-PDF 78-0315) appeared, as can be observed in Fig.1a. Presumably the CaO phase was the calcination product, but as the powder sample was in contact with ambient atmosphere after firing the product turned to $\text{Ca}(\text{OH})_2$ (as in Fig. 1a). Some small diffraction lines from CaO, (JCPDS-PDF 82-1691) and MgO, JCPDS-PDF 78-0430 can be also observed. After a successive and intensive milling process, and by treating the powder with phosphoric acid, next to the main lines of $\text{Ca}(\text{OH})_2$, new phases appeared (CaHPO_4 , JCPDS-PDF 01-0653) that are characteristic for sample A (Fig. 1b).

The morphological evolution of raw eggshell, calcinated at 900°C for 3 hours (Fig. 2a), followed by a mechanical activation (milling for 10 hours, Fig. 2b, sample A) and milled for 24 hours (Fig. 2c, sample B) are presented in Fig. 2. A lamellar nanostructure can be observed (consisting of 10-20 nm columns) in the case $\text{Ca}(\text{OH})_2$ as it was obtained after calcination (Fig. 2a). After mechanical activation for 10 hours this microstructure is characterised by 1-20 μm macrograins. This macrograins are consisting of adhered fine $\text{Ca}(\text{OH})_2$ and CaHPO_4 nanograins, as shown in Fig. 2b and observed by XRD investigations (sample A, in Fig. 1). After 10 hours a small quantity (sample A) was collected from jars. The milling process has been continued by adding another amount of phosphoric acid (the same quantity as the powder sample). As can be observed from Fig. 1c and Fig. 2c a totally new structure and morphology evolved after long milling. Micron size crystals of $\text{Ca}(\text{H}_2\text{PO}_4)_2 \cdot 2\text{H}_2\text{O}$ (JCPDS-PDF 70-0090) with hexagonal shape are characterising the sample B.

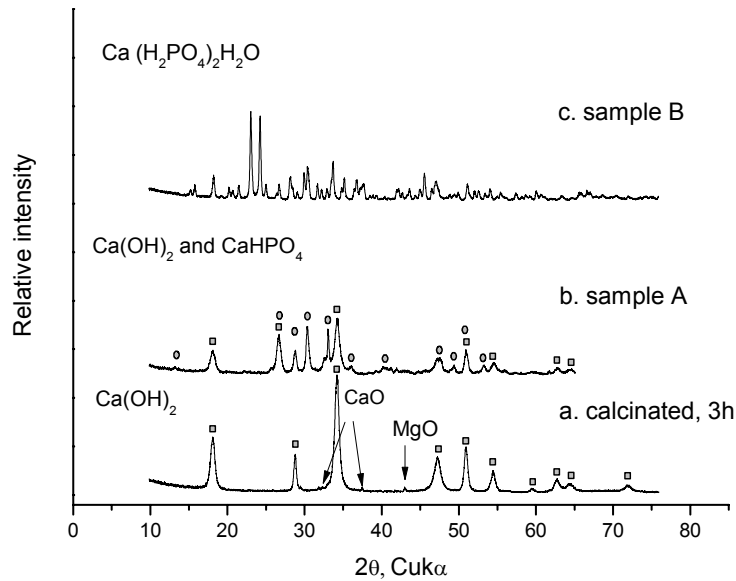


Fig. 1 X-ray diffractograms of powder samples. a) eggshell calcinated at 900°C for 3 hours, and exposed to ambient air after firing. b) the product after calcination, low acid/CaO ratio and short milling time, c) the product after calcination, high acid/CaO ratio and long milling time.

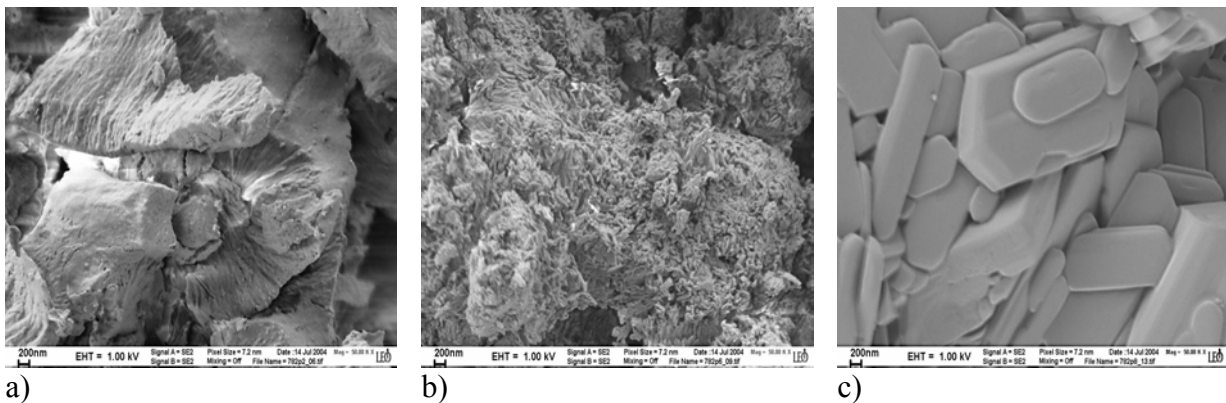


Fig. 2. Scanning electron micrographs of a) eggshell calcinated at 900°C for 3 hours. b) the product after calcination and 10h milling time, low acid/CaO ratio. c) the product after calcination and 24h milling time, high acid/CaO ratio.

As can be observed on Fig. 3a, after sintering at 900°C the sample A transformed to hydroxyapatite ($\text{Ca}_{10}(\text{PO}_4)_6(\text{OH})_2$), JCPDS-PDF 74-0565, noted as sample AS). Characteristic morphologies of sample AS and sample APS are presented in Fig. 4a and Fig. 4b. Coarsening of HAP grains can be observed, if a higher sintering temperature was applied (900°C and 1000°C). The samples, which resulted from a longer milling time (sample B) and with PEG (sample BPS) and carbon addition (BCPS), changed their morphology during sintering and resulted in the form of calcium-phosphate foams (Fig. 4c, 4d). As resulted, by carbon addition a more fine microstructure is obtained (Fig. 4d). X-ray diffraction analysis showed that the foams have $\beta\text{-Ca}(\text{PO}_3)_2$ structure (JCPDS-PDF 17-0500, Fig. 5a and 5b). The samples APS and APS-20 resulted from sintering of sample A at 1000°C have the same crystal structure as sample AS (Fig. 3). The sample APS-20 resulted from the same batch as the other APS sample, but during sintering it was placed next to the BCPS samples. The BCPS samples which have been sintered at 1000°C have burnt out during sintering and they condensed to the surface of the neighboring (APS-20) samples in form of micro- and nanocrystals (Fig. 6).

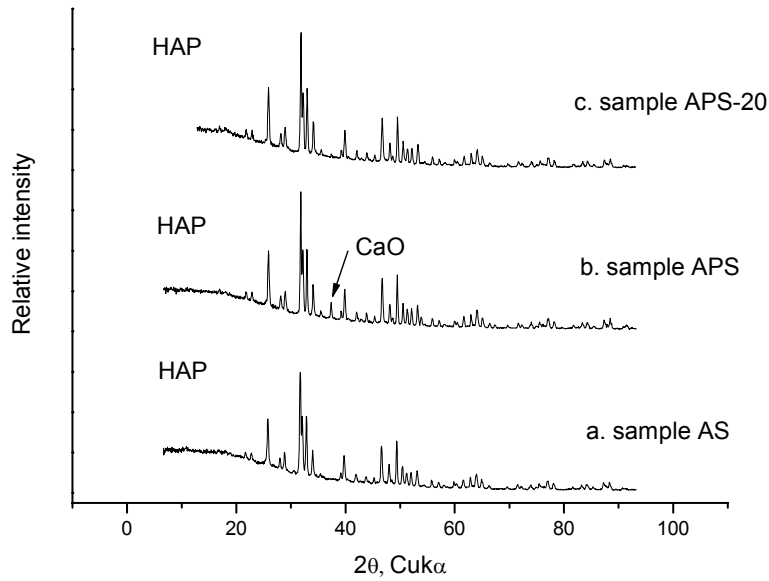


Fig. 3 X-ray diffractograms of sintered samples. a) sample AS. b) sample APS c) sample APS-20. The main lines of hydroxyapatite (HAP) can be recognized in the case of the all samples.

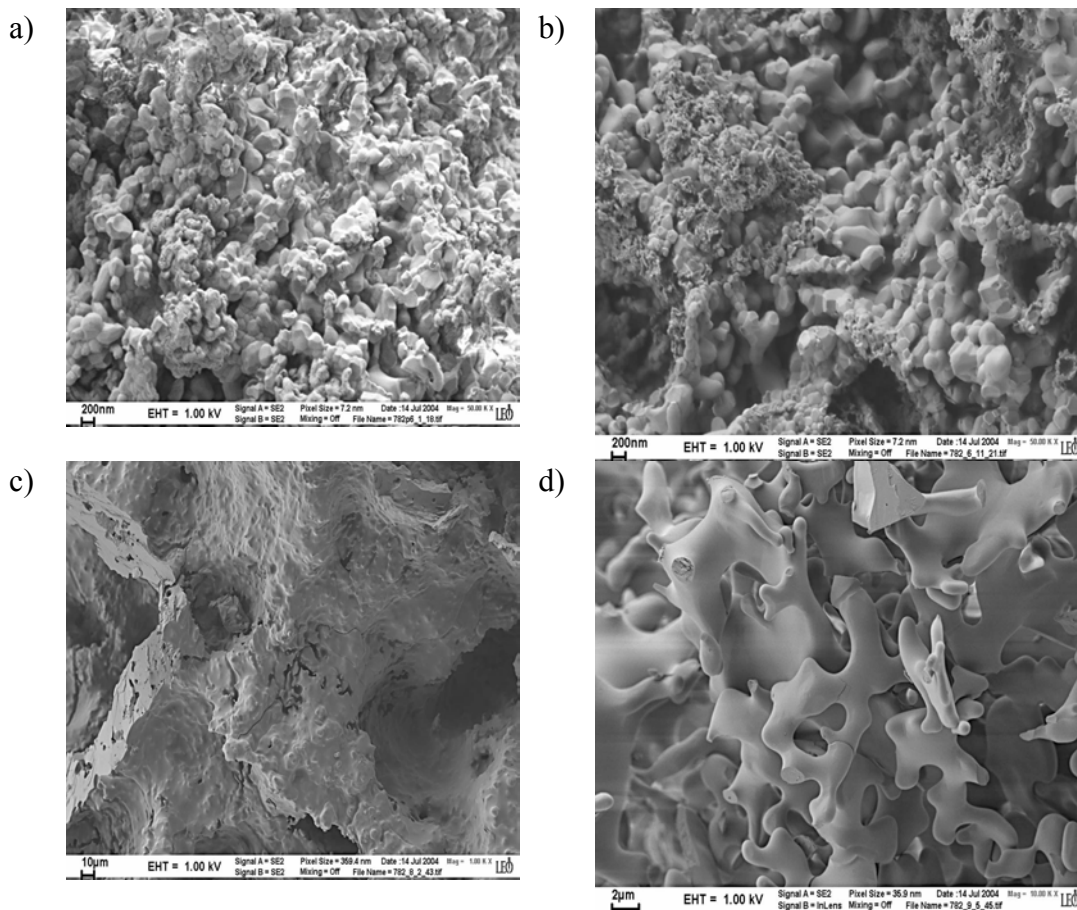


Fig. 4. Scanning electron micrographs of sintered samples a) nanocrystalline structure of sample AS (900°C, 2 hours). b) sample APS (1000°C, 2 hours). c) foam structure with 10-50 μm pores of sample BPS (900°C, 2 hours) and d) sample BCPS (900°C, 2 hours). Note the formation of foam structures in case of c) and d).

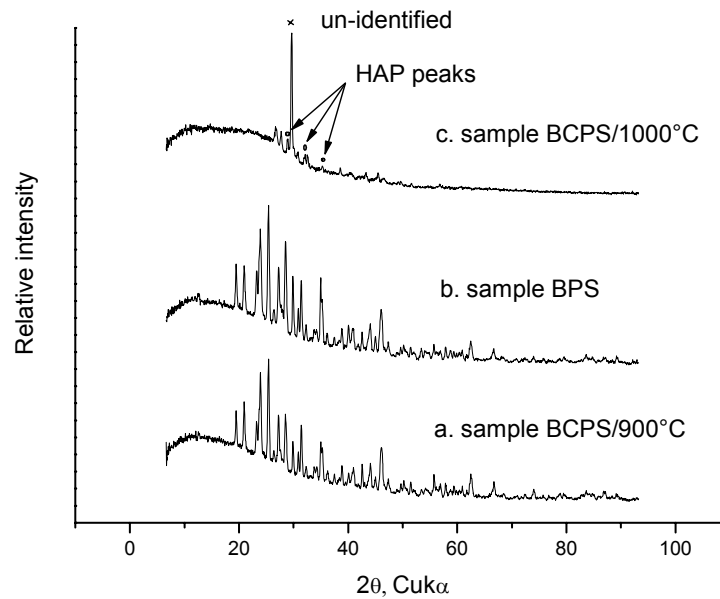


Fig. 5 X-ray diffractograms of sintered samples. a) sample BCPS/900°C. b) sample BPS. c) sample BCPS/1000°C.

A schematic view about the condensation process which took place in the presence of carbon can be followed in Fig. 6. First, the BCPS samples have grown in dimension, after that a self-combustion process took place and all of the BCPS samples have been evaporated. The condensation might have occurred from saturated vapour phase during cooling step to the neighboring surfaces. The as-obtained layer is very inhomogeneous as shown in Fig. 7.

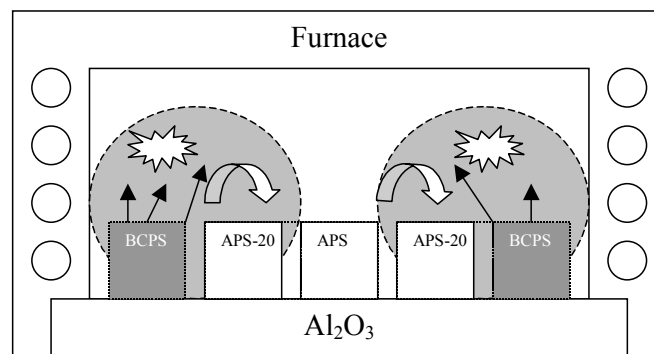


Fig. 6. A schematic view of condensation process.

Large grains with dimensions of 20-60 μm have condensed next to fracture surface (as in Fig. 7a). The surface of condensed grains is shown in Fig. 7b. As can be observed the big grains are consisting of small crystals with 1 μm length. Next to the bigger grains „small spots” with nanometer thickness can be observed which are well attached to the surface of sample APS-20 (as shown in Fig. 7c).

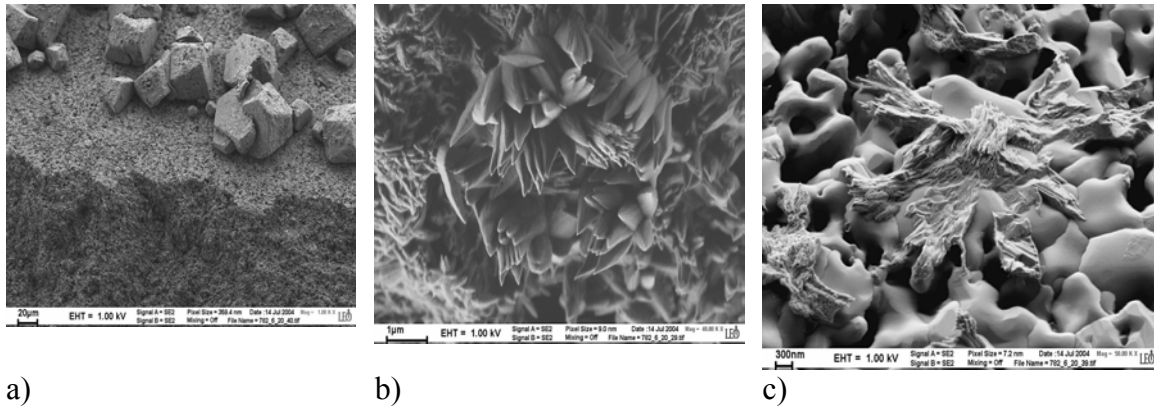


Fig. 7. Scanning electron micrographs of sintered BCPS sample a) large grains at fracture surface. b) the surface of grains. c) condensed spots connecting the grains of HAP surface.

The results of compositional analyses related to Ca/P atomic ratios made by total reflection X-ray fluorescence (TXRF) spectroscopy and prompt gamma activation analysis are presented in Table 2.

Table 2. Ca/P atomic ratios by total reflection x-ray fluorescence (TXRF) spectroscopy and prompt gamma activation analysis (PGAA)

Samples	TXRF	PGAA
AS	1.67	1.76
APS	-	1.74
BPS	0.11	0.43
BCPS	-	0.43

The TXRF spectra of the two sample are shown in Fig. 8. As it can be seen there is no other element in the sample apart from the main constituents. From the PGAA measurements we observed some Mg and S contamination. It can also be recognised that the BPS sample contains significantly smaller amount of Ca with respect to P. The quantitative evaluation of the spectra provides information about the atomic ratio of Ca and P. This ratio is well-known for the stoichiometrical hydroxyapatite, that is the AS sample: $Ca/P \approx 1.67$. The atomic ratio in the BPS sample is however significantly smaller: $Ca/P \approx 0.11$.

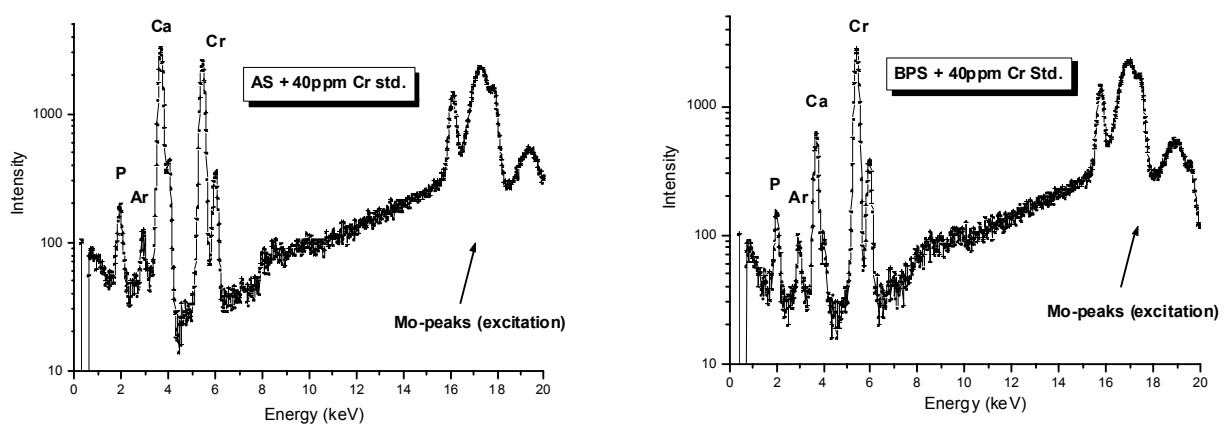


Fig. 8 TXRF spectra of the AS (left) and BPS (right) samples. Measurement live time was 100 s.

It should be noted that the dissolution was successful in the case of the AS sample, but the BPS sample was impossible to take up into solution. The lower peaks in the spectrum of the BPS sample are therefore a simple consequence of the lower solubility.

Conclusions

The processing route of calcium phosphate ceramics and the end product characteristics have been found to be influenced by acid/CaO mixing ratio, milling time and temperature of heat treatment applied. Calcium phosphate foams resulted at higher acid/CaO mixing ratio, longer milling time with high specific surface area. Samples with mono phase HAP have been obtained at lower acid/CaO mixing ratio and shorter milling. Compositional analyses showed that the Ca/P atomic ratios of the calcium phosphate foams are significantly smaller than for hydroxyapatite samples. At higher sintering temperatures calcium phosphate thin coatings have been realized with good adherence to HAP substrate.

Acknowledgements

Dr. Csaba Balázsi thanks for OTKA Postdoctoral Research Grant (D38478) and János Bolyai Research Grant.

References

- [1] E.M. Rivera, M. Araiza, W. Brostow, V.M. Castano, J.R. Diaz-Estrada, R. Hernandez, J.R. Rodriguez, *Materials Letters* 41 (1999) 128.
- [2] S.J. Lee, S.H. Oh, *Materials Letters* 57 (2003) 4570.
- [3] F. Peters, D. Reif, *Mat.-wiss. U. Werkstofftechn.* 35, No. 4 (2004) 203.
- [4] P. Seidel, E. Dingeldein, *Mat.-wiss u. Werkstofftech.*, 35, No. 4. (2004) 208.
- [5] B. Ben-Nissan, *Nanoceramics in biomedical applications*, MRS Bulletin, Vol.29, No.1 (2004)
- [6] Paul Ducheyne, W. Van Raemdonck, J. C. Heughebaert, M. Heughebaert, *Biomaterials*, 7 (1986) 97.
- [7] Ben-Nissan, A. Milev, R. Vago, *Biomaterials*, Vol. 25, Iss. 20, (2004) 4971.
- [8] J. L. Ong, L. C. Lucas, W. R. Lacefield, E. D. Rigney, 13 (1992) 249.
- [9] Y. W. Gu , K. A. Khor , D. Pan, P. Cheang, *Biomaterials*, Vol. 25, Iss. 16, (2004) 3177.
- [10] T. Kokubo, M. Hanakawa , M. Kawashita, M. Minoda, T. Beppu, T. Miyamoto, T. Nakamura, *Biomaterials*, Vol. 25, Iss. 18, (2004) 4485.
- [11] S. Kurunczi, Sz. T, J.W. Beal, *Journal of Radioanalytical and Nuclear Chemistry*, Vol. 253, No.2, (2002) 291-295.
- [12] www.ketek-gmbh.de
- [13] QXAS, IAEA Seibersdorf Laboratories, Austria, Version 3.5, 1996
- [14] Zs. Révay, G. L. Molnár, *Radiochim. Acta* 91. 361-369 (2003)